PROCEEDINGS, 41st Workshop on Geothermal Reservoir Engineering
Stanford University, Stanford, California, February 22-24, 2016
SGP-TR-209

3D analysis of geothermal fluid flow favorability: Brady's, Nevada, USA

Drew L. Siler[1], Nicholas H. Hinz[2], James E. Faulds[2] and John Queen[3]

[1]Earth Sciences Division, Lawrence Berkeley National Laboratory, Berkeley, CA 94720, USA

[2]Nevada Bureau of Mines and Geology, University of Nevada, Reno, Reno, NV 89557, USA

[3]HiQ Geophysical Inc. 106 Fairway Avenue, Ponca City, OK, 74601, USA

dlsiler@lbl.gov

Keywords: Structure, permeability, 3D modeling, geology, exploration

ABSTRACT

Geothermal circulation requires heat, permeability and fluids. Fracture permeability along discrete fault zones provides the pathways for fluid convection. Within individual faults, however, fluid flow zones can have variable character, size, and spatial distribution, representing a significant challenge to exploration and evaluation of geothermal resources. A comprehensive and validated methodology for quantitatively identifying the character, extent, and location of most likely fluid upflow zones within a resource area does not exist. Here, we present a methodology for evaluating favorability for geothermal fluid flow in 3D, an application of this technique to the Brady's geothermal system, Nevada, USA, and a preliminary evaluation of the results based on data from the production field. A variety of data types, including 2D seismic reflection data, downhole lithologic data, and geologic map data are integrated in 3D space in order to develop a 3D geologic model of the Brady's geothermal system. From this geologic model, the stress state of modeled faults, the density of fault intersections, and the inferred fluid flow characteristics of the various stratigraphic intervals are evaluated as proxies for permeability and geothermal fluid flow. Integration of these results with temperature data reveals locations within the geothermal field where the collocation of probable fracture permeability and high temperatures indicates a high likelihood for hosting geothermal fluid circulation. These results are consistent with the locations of injection, production, and non-productive wells within the Brady's field. Validation of these results with data from the well field suggests that these techniques do indeed shed light on specific details of the fluid flow systematics in geothermal systems. Though Brady's is a relatively data-rich system, this methodology can be adapted and applied to exploration and resource assessment not only in mature production fields, but also in blind, greenfield and otherwise data-poor geothermal areas.

1. INTRODUCTION

In geothermal fields high temperatures drive fluid circulation through permeable pathways in the crust. Fracture permeability associated with discrete fault zones is the primary form of permeability in many geothermal systems and is thus a key factor in controlling the location of exploitable fluid upwelling. Interconnected fault and fracture networks control the permeability pathways, but these pathways and the fluid upwelling zones that they host, can have very limited spatial extent, on the order of 10s-100s of meters of strike-length (Caine et al., 1996; Caine and Forster, 1999; Fairley et al., 2003; Fairley and Hinds, 2004; Mitchell and Faulkner, 2012; Meller and Kohl, 2014). Developing techniques for locating and characterizing these discrete areas in the subsurface that have the appropriate characteristics for fluid upwelling is critical in order to mitigate the risks and costs associated with drilling non-productive geothermal wells, and to continuing growth in utilization of this renewable energy resource.

The requisite first step in this methodology is accurate and precise characterization of the subsurface geology. Brady's is a relatively data-rich geothermal system. We integrate a variety of data types, including 2D seismic reflection data, downhole lithologic data, and geologic map data in order to develop a 3D geologic model of the Brady's geothermal system. Based on the 3D geologic model, a 3D map of the favorability for geothermal fluid upwelling throughout the field is built. This favorability analysis is based on evaluation of several proxies and direct indicators of heat, permeability, and fluids in the subsurface. The stress state of modeled faults, the density of fault discontinuities, and the fluid flow characteristics of the various stratigraphic intervals are evaluated as proxies for permeability. Temperature data are incorporated as direct indicators of the distribution of heat and as proxies for the occurrence of fluid circulation in the subsurface. Finally, we evaluate the results of the 3D geothermal favorability model by comparison with well data from the producing geothermal field.

Correlation between the results of the 3D geothermal favorability model and relative well productivity throughout the Brady's geothermal field suggests that the 3D favorability map is consistent with the characteristics and the spatial variability in fluid upwelling throughout the geothermal system. The validation of these results at Brady's indicates that these techniques are indeed viable for understanding fluid flow systematics in geothermal systems. These techniques can be extended and adapted for all stages of geothermal exploration and development, from early exploration and resource assessment to resource management and field maintenance.

2. 3D GEOTHERMAL FAVORABILITY MAPPING AT BRADY'S

The geothermal favorability mapping technique is based on similar concepts borrowed from 'play-fairway' exploration techniques utilized in the petroleum industry. While a geothermal system requires the collocation of heat, permeability and fluid, a petroleum system requires the geologic/tectonic conditions that generate source, reservoir, trap, seal, and a migration pathway to charge the reservoir with hydrocarbons (Baker et al., 1986; Doust, 2010). Prospective petroleum systems are identified based on the collocation of these elements in space. Similarly, geothermal play-fairway techniques have been used to evaluate geothermal favorability at the regional scale through comparison of the collocation of a variety of geothermal indicators (e.g. Faulds et al., 2015). 3D geothermal

favorability mapping is analogous, but applied locally, at the scale of an individual geothermal field or prospect. 3D geologic modeling and 3D geothermal favorability mapping are done using EarthVision software, by Dynamic Graphics.

The Brady's geothermal field, in northwestern, Nevada, USA has been the subject of geothermal exploration and development since 1959 and geothermal electricity production since 1992. The Brady's geothermal system supplies fluid to a power station with a total electricity production capacity of 26.4 MWe, as well as to a direct-use vegetable drying facility. Heat and permeability at Brady's are controlled by regionally high heat flow (Lachenbruch and Sass, 1977; Blackwell, 1983) and Basin and Range-style, Miocene-recent extensional faulting (Colgan et al., 2006; Faulds et al., 2010a). Brady's, like some ~32% of geothermal systems in the Great Basin, is controlled by a step-over in a normal fault system (Faulds et al., 2006; Faulds et al., 2010b; Faulds et al., 2011). The Brady's step-over occurs as a ~1-km wide left-step in the west-dipping, north-northeast-striking Brady's fault zone (Figure 1). Geothermal features along the Brady's fault zone include active fumaroles, sinter, calcium carbonate tufa and silicified sediments (Kratt et al., 2006). The Brady's area has also hosted historic geysers and hot springs. Equilibrated down hole fluid temperatures at Brady's are as high as 207°C (Shevenell et al., 2012).

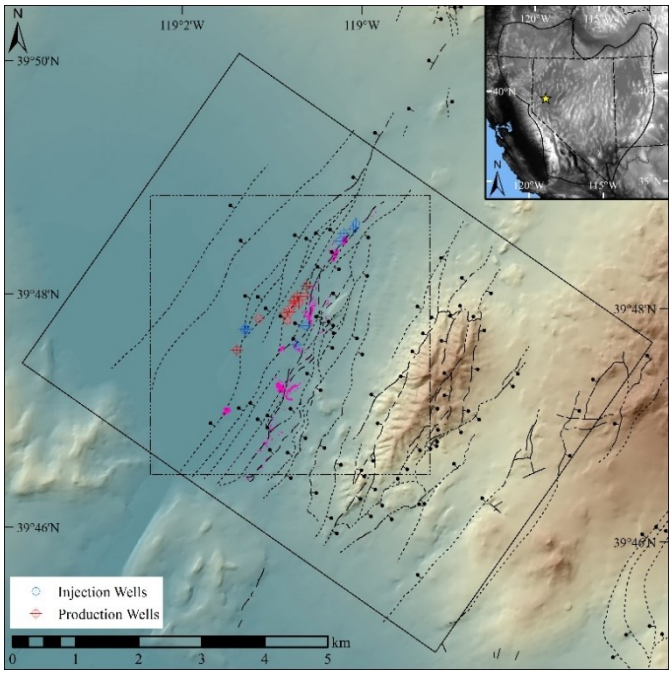

Figure 1. Fault map of the Brady's geothermal field from Faulds et al. (2012) and Faulds (unpublished data). Inset shows the location of the Brady's geothermal field within the Great Basin, western USA. Mapped geothermal surface features (Kratt et al., 2006; Faulds et al., 2012) are shown in pink. The solid rectangle indicates the extent of the 3D geologic model (Figure 2), the dashed square indicates the extent of Figures 6 and 7.

3. METHODS

3.1 3D Geologic modeling

We employ established 3D geologic modeling methods (Moeck et al., 2009; Jolie et al., 2012; Siler et al., 2012; Siler and Faulds, 2013; Siler et al., 2016) and expand upon 3D modeling at Brady's by Jolie et al., (2015). The Brady's 3D geologic model (Figure 2) was constructed based on 1:24,000 scale geologic mapping (Faulds et al., 2012), stratigraphy interpreted from lithologic analyses of cuttings and core from twenty-one wells, and interpretations of four seismic reflection profiles and four geologic cross-sections. For details on the seismic reflection data collection and processing, see the companion paper (Queen et al., 2016) in this volume.

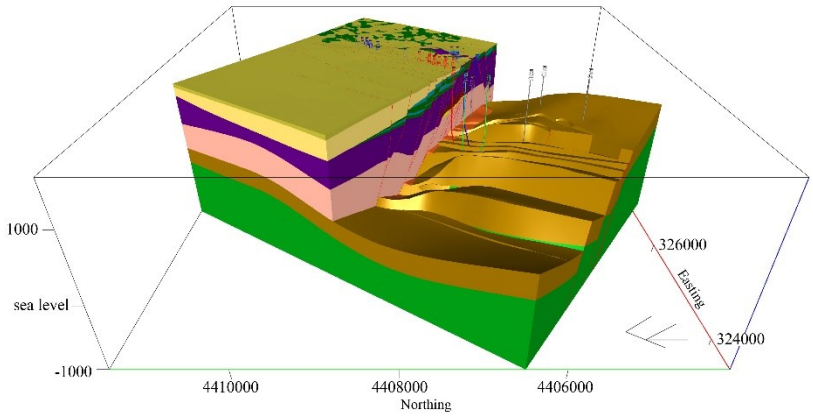

Figure 2. 3D geologic model for Brady's geothermal system. The model is sliced vertically through the Brady's step-over revealing a high density of faults within the step-over. Red and blue wells are production and injection wells. Green wells have been used for both production and injection. Grey wells are non-productive wells. All distances in meters. Image generated using EarthVision, Dynamic Graphics Inc., Alameda, CA.

3.2 Assessing uncertainty in the modeled geology

Uncertainty in the 3D modeled geology was evaluated based on relative distance between input data. Qualitatively, near to an input dataset, very low uncertainty in the modeled geology is expected, but uncertainty increases with distance. At progressively increasing distances, we have progressively higher uncertainty. Past a certain distance, however, where the data are of little use for constraining modeled geology, the progressive increase in uncertainty with distance decreases. Accordingly, a logarithmic curve is utilized to assess

relative uncertainty quantitatively (Figure 3 inset). There is zero relative uncertainty in the modeled results associated with a certain dataset directly adjacent to those data. The increase in relative uncertainty is adjusted relative to the mean fault spacing and mean stratigraphic thickness as defined by geologic modeling, which is ~250 m at Brady's. At 2× the mean stratigraphic thickness and fault spacing (by this distance for an input data set several faults or several stratigraphic contacts may have been crossed, and we would therefore have lower confidence in the modeled geologic interpretation based on those data) we have uncertainty, which we set to a relative uncertainty of 0.5 (Figure 3 inset). At great distances from input data, we have the highest uncertainty, a relative uncertainty rating of 1, in the modeled results. We calculate the relative uncertainty for each input dataset, (the seismic reflection profiles, geologic cross-sections, geologic map, and the well bores with lithologic data), and sum them such that we have an uncertainty rating, between one and four (four input datasets) for every location in the 3D geologic model (Figure 3). In areas where the relative uncertainty is high, the modeled geologic relationships are *consistent* with the input data, with local and regional geologic data, and with geologic principles, but the modeled geologic relationships are not particularly well *constrained* by the input data, relative to other parts of the model.

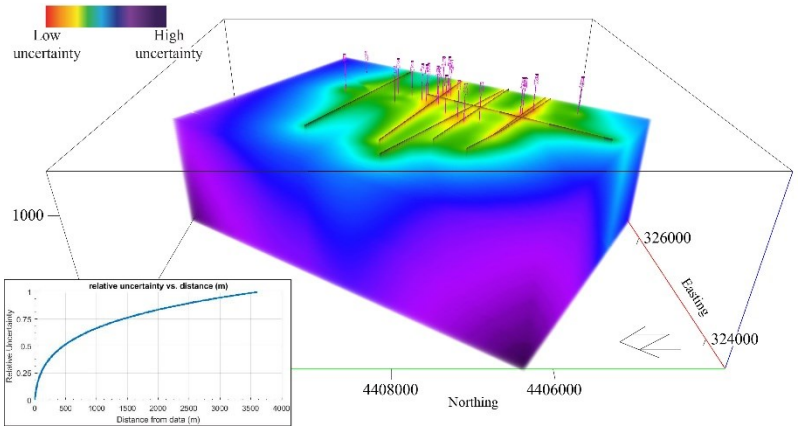

Figure 3. Relative uncertainty in the Brady's 3D geologic model. Uncertainty for each input data set, the seismic reflection profiles and geologic cross-sections (black planes), the well paths with analyzed core or well cuttings (in pink) and the geologic map (not show), is calculated based on the distance from those data and logarithmic relative uncertainty curve (inset). Cool colors correspond to low relative uncertainty, warm colors to high relative uncertainty. All distances in meters. Image generated using EarthVision, Dynamic Graphics Inc., Alameda, CA.

3.3 Geothermal favorability proxies

Based on the 3D geologic model, several proxies for geothermal fluid flow are evaluated. In any given fault zone, permeability can be highly spatially variable (Caine et al., 1996; Caine and Forster, 1999; Mitchell and Faulkner, 2012; Meller and Kohl, 2014), resulting in spatial variation in fluid upflow on scales as fine as 10s-100s of meters (Fairley et al., 2003; Fairley and Hinds, 2004). The distance from the fault core, total fault displacement, fault dip, the recency of slip, host rock lithology, alteration, fault length, and the local stress conditions can all effect permeability variation (Norton and Knapp, 1977; Brace, 1980; Anders and Wiltschko, 1994; Sibson, 1994; Caine et al., 1996; Sibson, 1996; Evans et al., 1997; Caine and Forster, 1999; Rawling et al., 2001; Mitchell and Faulkner, 2012; Meller and Kohl, 2014). Though permeability variation can be affected by any or all of these factors, here we evaluate the stress state of faults, the density of fault discontinuities and the host rock lithology as proxies for permeability variation throughout the Brady's geothermal field. Other factors, such as fault strike and dip variation are also incorporated, as they effect the stress state calculation. Fault length is also utilized as a constraint on fault zone thickness and the scale of fault discontinuities.

3.3.1 Fault zones

We assume that production-grade geothermal fluid flow at Brady's occurs only along discrete fault zones, which are the most probable locations of the highest temperature and sustained geothermal production (Blackwell et al., 1999; Richards and Blackwell, 2002). A fault zone was generated around each 3D modeled fault plane with a half-width of 15 m, symmetrically on either side of the fault plane. This distance corresponds to the distance from the fault core at which micro-fracture density asymptotically approaches zero (Scholz et al., 1993) for a ~2.5 km long fault, the approximate strike-length of the Brady's geothermal field (Figure 1). Though fault zone thickness and the magnitude of fracture permeability certainly varies between fault core, breccia zone and the damage zone within a fault zone as well (Shipton and Cowie, 2003; Kim et al., 2004), most fault zones at Brady's are exposed such that it was generally not possible to evaluate the effective dimensionality of fracture permeability zones along faults and between faults. We therefore start by assuming that fault zone width and fluid flow potential are uniform within all fault zones at Brady's and that all fault zones have sufficiently high fracture permeability to act as fluid flow conduits. Permeability and fluid flow favorability within modeled fault zones can subsequently be enhanced by high values in the fracture permeability proxies, the stress state of the fault, the distance from fault discontinuities, and the host rock lithology.

3.3.2 Fault intersections and fault tips

Tectonic stresses are concentrated at discontinuities along faults (Pollard and Aydin, 1988; Scholz et al., 1993). This results in a relatively higher density of secondary faults and fractures, and higher potential for fluid flow in these areas (Curewitz and Karson, 1997; Curewitz and Karson, 1998; Micklethwaite and Cox, 2004; Sheldon and Micklethwaite, 2007). Fault intersections and fault tips are two such discontinuities that are readily identifiable based on 3D geologic modeling. The locations of fault tips and intersections in the 3D geologic model were spatially registered and the density of intersections and tip-outs per unit area was calculated in 3D space (methods from Alberti, 2011). The radius of the 'breakdown region' at a fault tip, the area where fracturing is most dense, is proportional to 0.1 times the half-length of the fault (Pollard and Aydin, 1988; Scholz et al., 1993). We utilize this value to scale the 3D fault

intersection/tip model. Again, using the ~2.5 km strike length of the Brady's geothermal field, we set individual fault intersections and fault tips, to have radii of ~125 m. The fault intersection/tip density decreases linearly from a maximum at the intersection or tip, to zero at a distance of 125 m from the intersection or tip. The 3D intersection density model was normalized to values between 0 and 1, where 1 represents locations with highest fault intersection/tip density in the 3D modeled area and 0 represents areas with no fault intersections or fault tips, i.e. those areas farther than 125 m from any fault intersection or fault tip (Figure 4B).

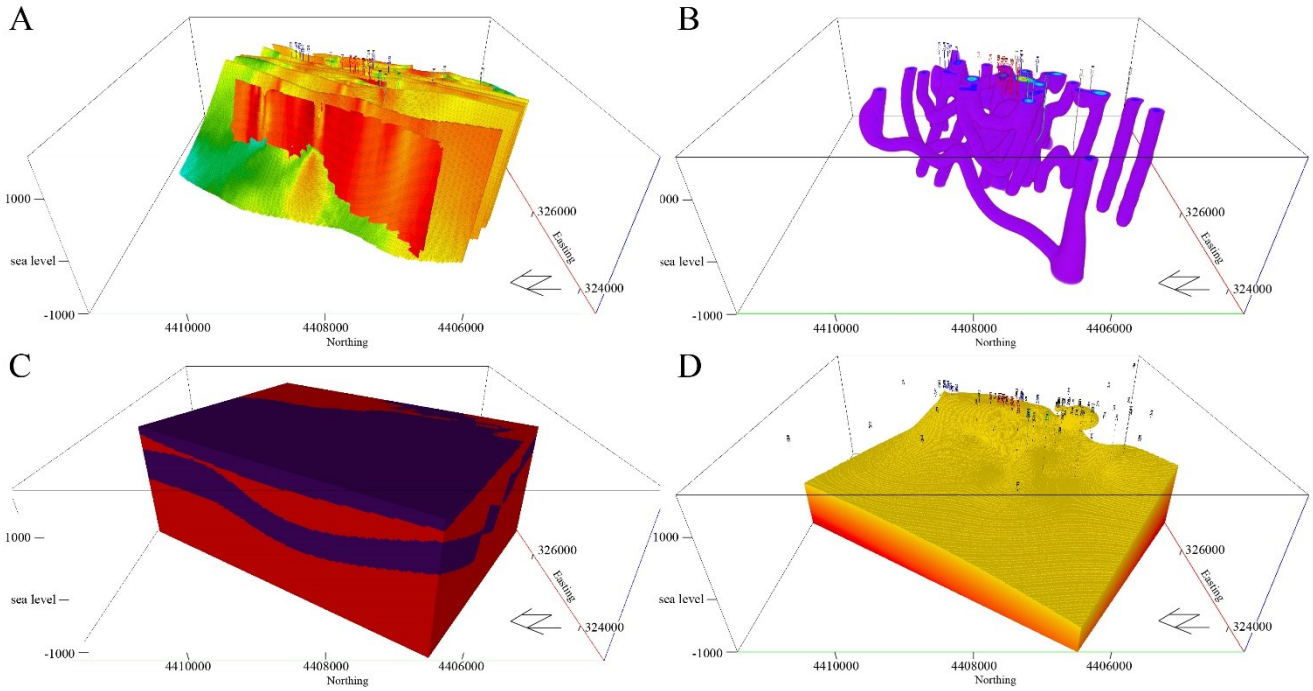

Figure 4. Geothermal favorability proxies at Brady's. Red and blue wells in all images are production and injection wells. Green wells have been used for both production and injection. Grey wells are non-productive wells. A) Dilation tendency variation along fault zones at Brady's. Warmer colors correspond to high dilation tendency and a high likelihood to be critically stressed and conduct fluid flow, cool colors correspond to low dilation tendency and a relatively lower likelihood to be critically stressed and conduct fluid flow. B) Fault intersection and fault tip density at Brady's. Warm colors correspond to high fault intersection/tip density, cool colors to low intersection/tip density. C) Favorable stratigraphic zones at Brady's. Red corresponds to favorable stratigraphic intervals as defined by the locations of flowing intervals in wells, purple corresponds to unfavorable stratigraphic intervals. D) Modeled 3D temperature at Brady's. Equilibrated downhole temperature measurements from the black wells were used to construct the model. Warm colors correspond to the highest temperature areas. The yellow surface shown is the 135°C isosurface, the lowest temperature fluid that have been produced at Brady's. All distances in meters. Image generated using EarthVision, Dynamic Graphics Inc., Alameda, CA.

3.3.3 Fault stress state

The degree that a fault zone is critically stressed under ambient stress conditions is an indicator of the potential of a fault to act as a conduit for fluid flow (Sibson, 1994; Barton et al., 1995; Morris et al., 1996; Sibson, 1996; Ito and Zoback, 2000; Townend and Zoback, 2000; Zoback and Townend, 2001). Independent of mechanical properties of the fault or the host rock, slip tendency (Morris et al., 1996) and dilation tendency (Ferrill et al., 1999) are calculated based on the resolved shear stress and normal stress on fault planes. In the tectonically active Great Basin, we can safely assume that most faults are sufficiently stressed such that slip and dilation tendency are appropriate representations for the relative critically stressed nature of the faults. Faults with relatively high slip or dilation tendency are more likely to be critically stressed and therefore are favorable for fluid upwelling.

Slip and dilation tendency were calculated for each 3D modeled fault plane based on the modeled geometry of the fault and the ambient stress conditions at Brady's. The minimum horizontal stress azimuth (S_{hmin}) is oriented 114°, with the maximum horizontal stress (S_{Hmax}) oriented 024°, and the maximum stress vertical (S_v). These azimuths, as well as the stress magnitudes used for slip and dilation tendency calculation are taken from a published stress model built based on analyses of borehole televiewer data from well 27-15 at Desert Peak, which is roughly ~7 km southeast of the Brady's geothermal field (Hickman and Davatzes, 2010). This stress model from nearby Desert Peak is consistent within error of the stress model calculated based on inversion of fault kinematic data from the northern Hot Springs Mountains (data from Faulds as described in Jolie et al., 2015), as well as drilling induced fracture data from well 15-12 within the Brady's field (Jolie et al., 2015). Regionally, the Brady's geothermal field lies in an area of predominantly east-southeast/west-northwest directed extension associated with Basin and Range-style tectonics (Colgan et al., 2006), so a normal faulting stress regime with S_{hmin} oriented 114° is consistent with regional data as well.

Slip and dilation tendency vary between values of 0, a fault plane oriented such that it has no resolved shear or normal stress and has no likelihood for slip or dilation, and 1, a fault plane that is ideally oriented for slip or dilation under ambient stress conditions. Each fault zone was populated with the calculated slip and dilation tendency values from the appropriate fault plane, resulting in 3D slip and dilation tendency models for the Brady's geothermal field (Figure 4A)

3.3.4 Host rock lithology

Some lithologies are more conducive to generation and maintenance of fracture permeability and hosting fluid flow than others (Hill, 1977; Sibson, 1994; Hinz et al., 2011). We do not have data regarding the competency variation in the lithologic section at Brady's. Instead, we interpret that all locations along the production or injection well paths that are reported as flowing intervals (based on publically available data, Nevada Division of Minerals) lie within lithologic units that are conducive to supporting extensive fracture permeability when faulted. We also interpret that stratigraphic units containing no flowing zones are not sufficiently competent to support fracture permeability and therefore are unfavorable for geothermal fluid flow.

The flowing zones and the 3D modeled stratigraphy indicate that the sections of the production and injection wellbores that flow are exclusively within a shallow ~500-meter-thick, section of late Miocene dacite and basalt lava flows and domes and a deeper ~1000-meter-thick section of Oligocene rhyolitic ash flow tuffs and the underlying Mesozoic basement. These two stratigraphic intervals are separated by a ~350 m-thick zone of Miocene andesite and dacite lavas, with interbedded lacustrine sediments, minor rhyolite lavas and tuffs, in which all production and injection wells are cased and no fluid flow was reported. We interpret that this intermediate stratigraphic zone and all other non-flowing lithologies throughout the Brady's area do not support fracture permeability or fluid flow to the same extent that the late Miocene dacite and basalt section and lower Oligocene rhyolitic tuff and Mesozoic basement sections. In the 3D geothermal favorability model, fault zones within these lithologies are capable of hosting fracture permeability and fluid flow, a favorability of 1, while fault zones within other lithologies in the stratigraphic section are not favorable for fluid flow, favorability of 0 (Figure 4C) .

3.3.5 Temperature and fluids

Discrete temperature anomalies in and around geothermal fields are commonly interpreted as indicators of heat transport via convection (e.g. by circulating fluids), a more efficient means of heat transport than conduction. Temperature data, therefore, are both direct indicators of the modern distribution of heat and a proxy for circulating fluids. Approximately 200 deep geothermal and shallow temperature gradient wells with equilibrated downhole temperature logs are publically available within and proximal to the Brady's geothermal field (Shevenell et al., 2012). Based on these data, a 3D temperature interpolation was constructed, using a minimum distance gridding algorithm, for the Brady's geothermal field. Monthly average production temperatures have ranged between 135-164°C throughout the lifetime of the Brady's field (based on publically available data, Nevada Division of Minerals). While the minimum temperature for production grade geothermal fluid flow is not only dependent on temperature, but also on fluid flow-rate, power plant design, and economics, among other things, we assume 135° is the lowest feasible production temperature in the Brady's field. Interpolated temperatures from 135° C to the maximum measured temperature of 207° C were normalized to values between 0 and 1 (Figure 4D).

3.3.6 Geothermal fluid flow favorability

The normalized 3D models for each proxy are summed, generating a 3D model for geothermal fluid flow favorability throughout the Brady's geothermal field. Values are normalized because we cannot constrain how, for instance, the potential for fluid flow along a critically stressed fault quantitatively relates to the potential for fluid flow at a fault intersection or to the potential for fluid flow indicated by a temperature anomaly. By normalizing and mathematically 'stacking' these semi-quantitative values we can highlight areas in the subsurface that are characterized by the highest degree of collocation of the four fluid flow proxies. The slip tendency model, dilation tendency model, and intersection density model were each incorporated with the lithology model, so that only areas within each model that occur within favorable stratigraphic zones have positive favorability ratings, whereas all areas within unfavorable lithologic intervals have a rating of 0. These models were added to the temperature model.

4. RESULTS

4.1 3D Geothermal favorability

The proxies and indicators for heat, permeability, and fluids reveal locations throughout the Brady's geothermal field that are most favorable for fluid flow. The 3D fault intersection/tip density model, for instance, defines a cluster of steeply- to moderately-dipping columns around single fault intersections/tips and larger, irregular volumes in locations where progressively more faults intersect and tip out (Figure 4B). These areas are likely to be characterized by a relatively high density of faults and fractures. This result is consistent with findings of spatially-discrete, high-permeability flow-paths in a variety of other geothermal settings (Caine et al., 1996; Curewitz and Karson, 1997; Gudmundsson, 2000; Fairley et al., 2003; Fairley and Hinds, 2004). Stress analysis based on the stress conditions within and local to the Brady's field (Hickman and Davatzes, 2010; Jolie et al., 2015) indicates that, steeply-dipping (70°+) north-northeast-striking fault segments have the highest tendency for dilation, whereas moderately dipping (30-60°) north-northeast-striking faults have the highest tendency for slip. Thus, fault segments within the Brady's geothermal field that are most favorably oriented to act as fluid flow conduits, strike north-northeast and dip either moderately or steeply to the west (e.g. Figure 4A). The lithologic model constrains the most favorable areas for geothermal fluid to two distinct lithologic zones, the upper zone is ~500 m thick, while the lower zone extends to the base of the 3D modeled volume (Figure 4C). These two zones are separated by a ~350 m-thick zone of low geothermal fluid flow favorability. Temperature data reveal relatively high, production grade temperatures (>135° C) extending to the shallow subsurface (100 m depth) in a zone that is ~2 km long in the along-fault-strike direction and ~1 km in the across-fault-strike

direction and within the Brady's step-over (Figure 4D). Distal to the Brady's step-over, temperatures greater than 135° C occur below ~1700 m depth.

Geothermal favorability ratings are higher within the Brady's step-over than in areas distal to the step-over (Figure 5 and 7). This is consistent with existing conceptual models of fracture permeability and geothermal fluid flow focused within step-overs and other complex structural interaction areas (Curewitz and Karson, 1997; Faulds et al., 2006; Faulds et al., 2011). Our results however, reveal the locations of discrete fault segments within the Brady's step-over that have the highest collocation of favorable geologic attributes and lie within the areas of highest temperature. These locations have a relatively higher likelihood for conducting geothermal upwelling relative to other areas within the step-over and throughout the rest of the field (Figure 5).

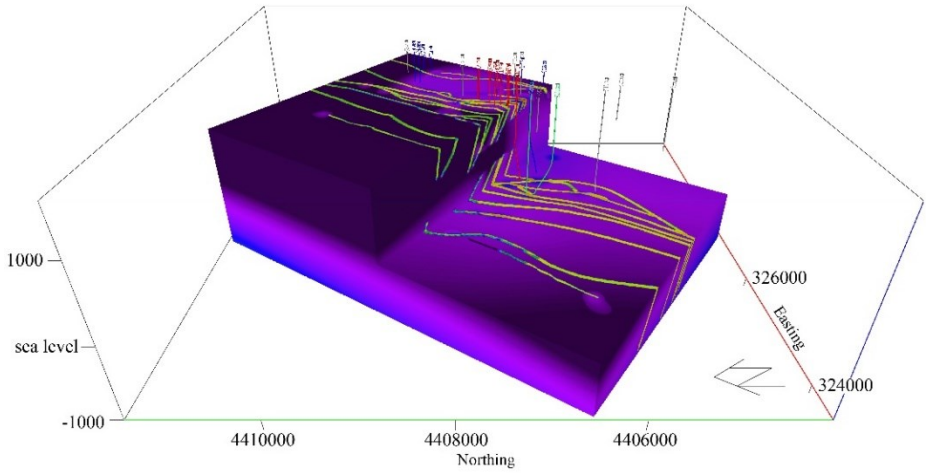

Figure 5. 3D geothermal favorability model (dilation tendency + slip tendency + intersection density + lithology + temperature) for Brady's. Red and blue wells are production and injection wells. Green wells have been used for both production and injection. Grey wells are non-productive wells. Warm colors correspond to high collocation of the four geothermal favorability proxies, and therefore high favorability for geothermal upwelling. Cool colors correspond to low favorability. All distances in meters. Image generated using EarthVision, Dynamic Graphics Inc., Alameda, CA.

4.2 Validation of 3D favorability results

Based on the 3D favorability map, the mean geothermal favorability rating for vertical well paths throughout the modeled area was calculated. Of these hypothetical vertical well paths, the highest favorability rating lies within the Brady's step-over and within ~350 m of wells 27-1-RD1 and 82A-11-RD3 (Figure 6), which have been the most prolific production wells throughout the life of the Brady's field from the 3D geothermal favorability map. Additionally, these hypothetical wells lie in an area that has very low relative uncertainty in the modeled geology.

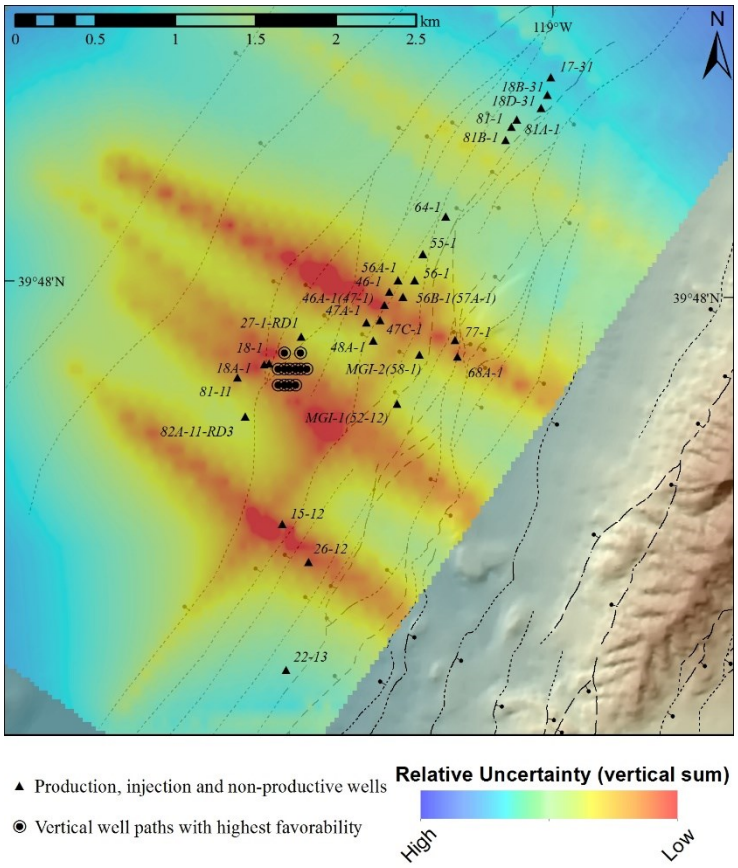

Figure 6. The locations of hypothetical vertical well paths with the highest geothermal favorability (circled points). These wells lie at the southern jog in the Brady's step-over and are within ~350 meters of wells 82A-11RD3 and 27-1-RD1, the two most prolific production wells at Brady's. The vertical sum of relative uncertainty is shown, the hypothetic vertical wells with the highest favorability also are associated with low relative uncertainty in the geologic model. Image generated using EarthVision, Dynamic Graphics Inc., Alameda, CA.

Geothermal production at Brady's has been ongoing since 1992. Between 1992 and 2013, nineteen wells within the Brady's geothermal field have been used in conjunction with electricity generation, twelve wells for production and nine for injection. Two wells have been used for both injection and production (based on publically available data, Nevada Division of Minerals). Nine wells within the Brady's field that have not been used for either production or injection, i.e. non-productive wells, were selected for comparison of the modeled favorability versus the actual production and injection wells. The summed favorability rating is calculated for each well path, and divided by the total length of the well path.

Each well, therefore has a well-length-normalized rating of geothermal favorability. The most favorable wells occur within and local to the Brady's step-over, whereas wells around the margin and outside of the step-over tend to be less favorable (Figure 7A). The mean favorability rating for production wells is higher than both the non-productive wells and injection wells (Figure 7B).

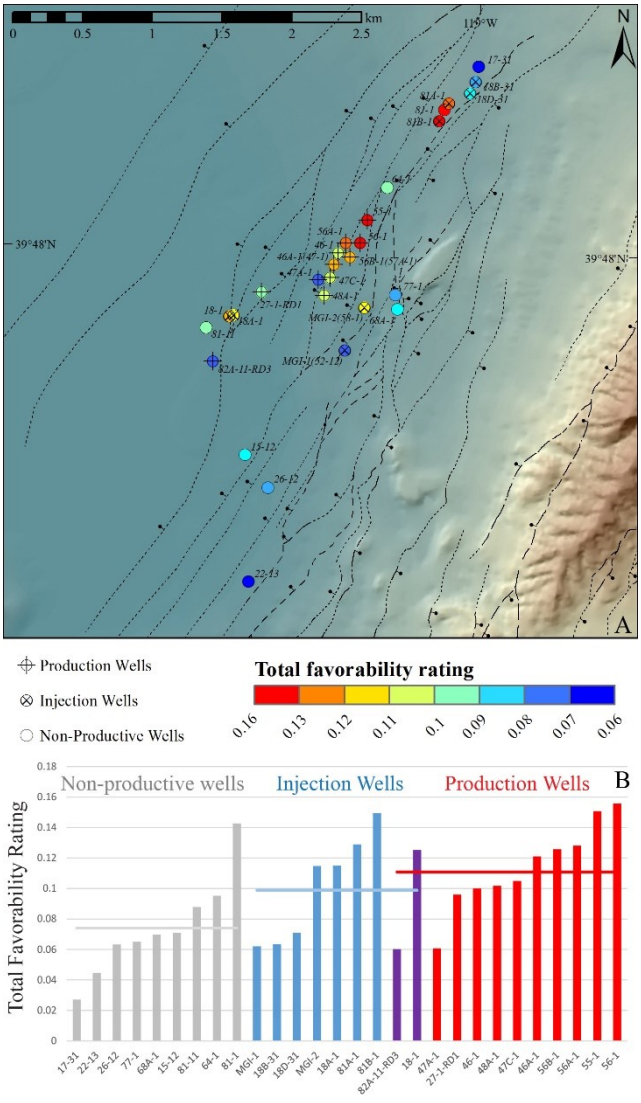

Figure 7. Geothermal favorability rating for wells in the Brady's geothermal field. Well favorability ratings (dilation tendency + slip tendency + intersection density + lithology + temperature) are the summed ratings from the 3D geothermal favorability map along each well path and are normalized to the length of the well. A) Wells within the left step-over in the Brady's fault zone generally have higher ratings then wells around the periphery of the step-over and outside of the step-over. B) The mean favorability rating (horizontal lines) for the wells that have been used for production (red) is higher than wells that have been used for injection (blue) and non-productive wells (grey). Purple wells have been used for both production and injection.

5. CONCLUSIONS

Geothermal energy will be an important component of the future energy production in the United States. Though geothermal systems may be indicated by a variety of surface and subsurface data sets, geothermal resources are discovered by drilling. A key aspect, therefore, to any geothermal exploration strategy is a methodology for selecting the most favorable drilling targets within a known or prospective resource area. A detailed and accurate model of the subsurface geological and structural geometries is a requirement. Accurate and precise 3D geologic modeling allows for definition of detailed and complex fault and stratigraphic structure. We show that the stress state of faults, the density of structural discontinuities, the fluid flow potential of various stratigraphic sequences, and the modeled temperature can serve as proxies for the favorability for geothermal fluid flow throughout the field. Applied at Brady's, these methods reveal discrete fault segments within the broad thermal anomaly with relatively high favorability for hosting geothermal upwelling. These 3D geothermal favorability results are consistent with data from the actively producing geothermal field. The validation of the 3D geothermal favorability results with well data from the producing geothermal field indicates that these methods do indeed shed light on the geologic controls of fluid upwelling and can be applied to geothermal systems for use in exploration, resource assessment, and resource management purposes.

ACKNOWLEDGEMENTS

We thank Ormat Technologies Inc. for their cooperation and input into this work. The analysis of the Brady's system was supported by Ormat and the U.S. Department of Energy under award DE-FG36-08GO18200 and DE-FG36-02ID14311 to Ormat Technologies, Inc. The assistance and advice of Robert McFaul at Dynamic Graphics Inc., Alameda CA in development of the 3D geothermal favorability mapping workflow, and Alan Morris for his assistance with 3D Stress, were instrumental to this paper. This work was also supported by Lawrence Berkeley National Laboratory under U.S. Department of Energy, Assistant Secretary for Energy Efficiency and Renewable Energy, Geothermal Technologies Program under the U.S. Department of Energy contract number DE-AC02-05CH11231.

REFERENCES

Alberti, M., 2011, 3D point cloud density calculation: a C++ program.

Anders, M.H., and Wiltschko, D. V, 1994, Microfracturing, paleostress and the growth of faults: Journal of Structural Geology, v. 16, no. 6, p. 795–815, doi: 10.1016/0191-8141(94)90146-5.

Baker, R.A., Gehman, H.M., James, W.R., and White, D.A., 1986, Geologic field number and oil and gas plays, in Rice, D.D. ed., Oil and Gas Assessment-Methods and applications: AAPG studies in Geology, p. 25–31.

Barton, C.A., Zoback, M.D., and Moos, D., 1995, Fluid flow along potentially active faults in crystalline rock: Geology, v. 23, no. 8, p. 23–27, doi: 10.1130/0091-7613(1995)023<0683.

Bibby, H.M., Caldwell, T.G., Davey, F.J., and Webb, T.H., 1995, Geophysical evidence on the structure of the Taupo Volcanic Zone and its hydrothermal circulation: Journal of Volcanology and Geothermal Research, v. 68, no. 1-3, p. 29–58, doi: 10.1016/0377-0273(95)00007-H.

Blackwell, D.D., 1983, Heat flow in the northern Basin and Range province: Geothermal Resources Council, Special Report 13, p. 81–93.

Blackwell, D.D., Wisian, K.W., Benoit, W.R., and Gollan, B., 1999, The Dixie Valley Geothermal System, a "Typical" Basin and Range Geothermal System, From Thermal and Gravity Data: Geothermal Resources Council Transactions, v. 23, p. 525–531.

Brace, W.F., 1980, Permeability of crystalline and argillaceous rocks: International Journal of Rock Mechanics and Mining Sciences Abstracts, v. 17, p. 241–251.

Caine, J.S., Evans, J.P., and Forster, C.B., 1996, Fault zone architecture and permeability structure: Geology, doi: 10.1130/0091-7613(1996)024<1025.

Caine, J.S., and Forster, C.B., 1999, Fault Zone Architecture and Fluid Flow : Insights From Field Data and Numerical Modeling:.

Colgan, J.P., Dumitru, T. a., Reiners, P.W., Wooden, J.L., and Miller, E.L., 2006, Cenozoic Tectonic Evolution of the Basin and Range Province in Northwestern Nevada: American Journal of Science, v. 306, no. 8, p. 616–654, doi: 10.2475/08.2006.02.

Curewitz, D., and Karson, J.A., 1998, Geological Consequences of Dike Intrusion at Mid-Ocean Ridge Spreading Centers, in Buck, W.R. ed., Faulting and Magmatism at Mid-Ocean Ridges, Geophysical Monograph 106, American Geophysical Union, p. 117–136.

Curewitz, D., and Karson, J.A., 1997, Structural settings of hydrothermal outflow: Fracture permeability maintained by fault propagation and interaction: Journal of Volcanology and Geothermal Research, v. 79, no. 3-4, p. 149–168, doi: 10.1016/S0377-0273(97)00027-9.

Doust, H., 2010, The exploration play: What do we mean by it? AAPG Bulletin, v. 94, no. 11, p. 1657–1672, doi: 10.1306/06301009168.

Evans, J.P., Forster, C.B., and Goddard, J. V, 1997, Permeability of fault-related rocks, and implications for hydraulic structure of fault zones: Journal of Structural Geology, v. 19, no. 11, p. 1393–1404, doi: 10.1016/S0191-8141(97)00057-6.

Fairley, J.P., Heffner, J., and Hinds, J., 2003, Geostatistical evaluation of permeability in an active fault zone: Geophysical Research Letters, v. 30, no. 18, doi: 10.1029/2003GL018064.

Fairley, J.P., and Hinds, J.J., 2004, Rapid transport pathways for geothermal fluids in an active Great Basin fault zone: Geology, v. 32, no. 9, p. 825–828, doi: 10.1130/G20617.1.

Faulds, J.E., Coolbaugh, M.F., Benoit, W.R., Oppliger, G.L., Perkins, M., Moeck, I., and Drakos, P.S., 2010a, Structural Controls of Geothermal Activity in the Northern Hot Springs Mountains, Western Nevada: The Tale of Three Geothermal Systems (Brady's, Desert Peak, and Desert Queen): Geothermal Resources Council Transactions, v. 34, p. 675–684.

Faulds, J.E., Coolbaugh, M.F., Vice, G.S., and Edwards, M.L., 2006, Characterizing Structural Controls of Geothermal Fields in the Northwestern Great Basin: A Progress Report: Geothermal Resources Council Transactions, v. 30, p. 69–76.

Faulds, J.E., Hinz, N.H., Coolbaugh, M.F., Cashman, P.H., Kratt, C., Dering, G.M., Edwards, J., Mayhew, B., and Mclachlan, H., 2011, Assessment of Favorable Structural Settings of Geothermal Systems in the Great Basin, Western USA: Geothermal Resources Council Transactions, v. 35, p. 777–784.

Faulds, J.E., Moeck, I., Drakos, P.S., and Zemach, E., 2010b, Structural Assessment and 3D geologic modeling of the Brady's geothermal area, Churchill County (Nevada, USA): A preliminary report, in Proceedings, Thirty-Fifth Workshop on Geothermal Reservoir Engineering, Stanford University, p. 298–302.

Faulds, J.E., Ramelli, A.R., Garside, L.J., Coolbaugh, M.F., and Green, H.L., 2012, Preliminary geologic map of the Desert Peak Quadrangle, Churchill County, Nevada: Nevada Bureau of Mines and Geology Open-File Report 12-5, scale 1:24,000:.

Ferrill, D.A., Winterle, J., Wittmeyer, G., Sims, D., Colton, S., Armstrong, A., Horowitz, A.S., Meyers, W.B., and Simons, F.F., 1999, Stressed rock strains groundwater at Yucca Mountain, Nevada: GSA Today, v. 9, no. 5, p. 2–9.

Flóvenz, Ó.G., and Sæmundsson, K., 1993, Heat flow and geothermal processes in Iceland: Geothermics, v. 225, p. 123–138.

Gudmundsson, A., 2000, Active fault zones and groundwater flow: Geophysical Research Letters, v. 27, no. 18, p. 2993–2996, doi: 10.1029/1999GL011266.

Hickman, S.H., and Davatzes, N.C., 2010, In-situ stress and fracture characterization for planning of an EGS stimulation in the Desert Peak Geothermal Field, Nevada, in Proceedings, Thirty-Fifth Workshop on Geothermal Reservoir Engineering, Stanford University, p. 13.

Hinz, N.H., Faulds, J.E., and Siler, D.L., 2013, Developing Systematic Workflow From Field Work to Quantitative 3D Modeling for Successful Exploration of Structurally Controlled Geothermal Systems: Geothermal Resources Council Transactions, v. 37, p. 275–279.

Ito, T., and Zoback, M.D., 2000, Fracture permeability and in situ stress to 7 km depth in the KTB Scientific Drillhole: Geophysical Research Letters, v. 27, no. 7, p. 1045–1048.

Jolie, E., Faulds, J.E., and Moeck, I., 2012, The Development of a 3D structural-geological model as part of the geothermal exploration strategy - A case study from the Brady's geothermal system, Nevada, USA, in Proceedings, Thirty-Seventh Workshop on Geothermal Reservoir Engineering, Stanford University, p. 421–425.

Jolie, E., Moeck, I., and Faulds, J.E., 2015, Quantitative structural–geological exploration of fault-controlled geothermal systems—A case study from the Basin-and-Range Province, Nevada (USA): Geothermics, v. 54, p. 54–67, doi: 10.1016/j.geothermics.2014.10.003.

Kim, Y.-S., Peacock, D.C.P., and Sanderson, D.J., 2004, Fault damage zones: Journal of Structural Geology, v. 26, no. 3, p. 503–517, doi: 10.1016/j.jsg.2003.08.002.

Kratt, C., Calvin, W., and Coolbaugh, M.F., 2006, Geothermal exploration with Hymap hyperspectral data at Brady–Desert Peak, Nevada: Remote Sensing of Environment, v. 104, no. 3, p. 313–324, doi: 10.1016/j.rse.2006.05.005.

Lachenbruch, A.H., and Sass, J.H., 1977, Heat flow in the United States and the thermal regime of the crust, in Heacock, J.G. ed., The Nature and Physical Properties of the Earth's Crust, American Geophysical Union Monograph, p. 626–675.

Meller, C., and Kohl, T., 2014, The significance of hydrothermal alteration zones for the mechanical behavior of a geothermal reservoir: Geothermal Energy, v. 2, no. 1, p. 12, doi: 10.1186/s40517-014-0012-2.

Micklethwaite, S., and Cox, S.F., 2004, Fault-segment rupture, aftershock-zone fluid flow, and mineralization: Geology, v. 32, no. 9, p. 813–816, doi: 10.1130/G20559.1.

Mitchell, T.M., and Faulkner, D.R., 2012, Towards quantifying the matrix permeability of fault damage zones in low porosity rocks: Earth and Planetary Science Letters, v. 339-340, p. 24–31, doi: 10.1016/j.epsl.2012.05.014.

Moeck, I., Schandelmeier, Æ.H., and Holl, H., 2009, The stress regime in a Rotliegend reservoir of the Northeast German Basin: International Journal of Earth Sciences, v. 98, p. 1643–1654, doi: 10.1007/s00531-008-0316-1.

Morris, A., Ferrill, D.A., and Henderson, D.B., 1996, Slip-tendency analysis and fault reactivation: Geology, v. 24, no. 3, p. 275–278.

Norton, D., and Knapp, R., 1977, Transport phenomena in hydrothermal systems; the nature of porosity: American Journal of Science, v. 277, no. 8, p. 913–936.

Pollard, D.D., and Aydin, A., 1988, Progress in understanding jointing over the past century Progress in understanding jointing over the past century: Geological Society of America Bulletin, v. 100, no. 8, p. 1181–1204, doi: 10.1130/0016-7606(1988)100<1181.

Rawling, G.C., Goodwin, L.B., and Wilson, J.L., 2001, Internal architecture, permeability structure , and hydrologic significance of contrasting fault-zone types: Geology, doi: 10.1130/0091-7613(2001)029<0043.

Richards, M.C., and Blackwell, D.D., 2002, A Difficult Search: Why Basin and Range Systems are Hard to Find: Geothermal Resources Council Bulletin, v. 31, no. 4, p. 143–146.

Rowland, J. V, and Sibson, R.H., 2004, Structural controls on hydrothermal flow in a segmented rift system, Taupo Volcanic Zone, New Zealand: Geofluids, v. 4, no. 4, p. 259–283, doi: 10.1111/j.1468-8123.2004.00091.x.

Scholz, C.H., Dawers, N.H., Yu, J., Anders, M.H., and Cowie, P.A., 1993, Fault Growth and Fault Scaling Laws: Preliminary Results: Journal of Geophysical Research, v. 98, no. B12, p. 951–961.

Sheldon, H.A., and Micklethwaite, S., 2007, Damage and permeability around faults: Implications for mineralization: Geology, v. 35, no. 10, p. 903–906, doi: 10.1130/G23860A.1.

Shervais, J., Glen, J., Liberty, L., Dobson, P., Gasperikova, E., Sonnenthal, E., Visser, C., Nielson, D., Garg, S., Evans, J., Siler, D., DeAngelo, J., Athens, N., and Burns, E., 2015, Snake River Plain Play Fairway Analysis – Phase 1 Report: Geothermal Resources Council Transactions, v. 39.

Shevenell, L.A., Oppliger, G., Coolbaugh, M.F., and Faulds, J.E., 2012, Bradys (Nevada) InSAR Anomaly Evaluated With Historical Well Temperature and Pressure Data: Geothermal Resources Council Transactions, v. 36, p. 1383–1390.

Shipton, Z.K., and Cowie, P.A., 2003, A conceptual model for the origin of fault damage zone structures in high-porosity sandstone: Journal of Structural Geology, v. 25, p. 333–344.

Sibson, R.H., 1994, Crustal stress , faulting and fluid flow, in Parnell, J. ed., Geofluids: Origin, Migration and Evolution of Fluids in Sedimentary Basins, Geological Society, London, Special Publications, p. 69–84.

Sibson, H., 1996, Structural permeability of fluid-driven fault-fracture: Journal of Structural Geology, v. 18, no. 8, p. 1031–1042.

Siler, D.L., and Faulds, J.E., 2013, Three-Dimensional Geothermal Fairway Mapping : Examples From the Western Great Basin, USA: Geothermal Resources Council Transactions, v. 37, p. 327–332.

Siler, D.L., Faulds, J.E., Mayhew, B., and Mcnamara, D.D., 2016, Geothermics Analysis of the favorability for geothermal fluid flow in 3D: Astor Pass geothermal prospect, Great Basin, northwestern Nevada, USA: Geothermics, v. 60, p. 1–12, doi: 10.1016/j.geothermics.2015.11.002.

Siler, D.L., Mayhew, B., and Faulds, J.E., 2012, Three-Dimensional Geologic Characterization of Geothermal Systems: Astor Pass, Nevada, USA: Geothermal Resources Council Transactions, v. 36, no. 2012, p. 783–786.

Townend, J., and Zoback, M.D., 2000, How faulting keeps the crust strong: Geology, v. 28, no. 5, p. 399–402, doi: 10.1130/0091-7613(2000)28<399:HFKTCS>2.0.CO.

Wallis, I.C., Mcnamara, D., Rowland, J. V, and Massiot, C., 2012, The nature of fracture permeability in the basement greywacke at Kawerau geothermal field, New Zealand, in Proceedings, Thirty-Seventh Workshop on Geothermal Reservoir Engineering, Stanford University, p. 232–240.

Zoback, M.D., and Townend, J., 2001, Implications of hydrostatic pore pressures and high crustal strength for the deformation of intraplate lithosphere: Tectonophysics, v. 336, no. 1-4, p. 19–30, doi: 10.1016/S0040-1951(01)00091-9.